Soft Matter

Simultaneous Control of Gaussian Curvature and Buckling Direction by Swelling of Asymmetric Trilayer Hydrogel Hybrids

Journal:	*Soft Matter*
Manuscript ID	SM-ART-09-2019-001922.R1
Article Type:	Paper
Date Submitted by the Author:	30-Nov-2019
Complete List of Authors:	Jeon, Seog-Jin; Kumoh National Institute of Technology, Polymer Science and Engineering Hayward, Ryan; University of Massaschusetts, Polymer Science and Engineering

SCHOLARONE™
Manuscripts

Please do not adjust margins

Journal Name

ARTICLE

Simultaneous Control of Gaussian Curvature and Buckling Direction by Swelling of Asymmetric Trilayer Hydrogel Hybrids

Seog-Jin Jeon[a,b] and Ryan C. Hayward[b,*]

Received 00th January 20xx,
Accepted 00th January 20xx

DOI: 10.1039/x0xx00000x

www.rsc.org/

Trilayer polymer films consisting of a thermoresponsive hydrogel, poly(diethyl acrylamide) (PDEAM), sandwiched by rigid layers of a glassy polymer, poly(*para*-methylstyrene) (P*p*MS), patterned into parallel striped features are prepared and used to drive temperature-responsive reversible anisotropic expansion. Significant swelling occurs along the direction perpendicuar to the stripes, while very little swelling is observed along the direction parallel to the stripes, leading to an overall swelling anisotropy of 1.17. Introducing a difference Δ in the widths of the stripes on the top to bottom surfaces causes the films to roll upon swelling, where both the magnitude and sign of the resulting curvature can be controlled by varying Δ. Using patterns of concentric circular lines (analagous to +1 defects in liquid crystalline polymers), we demonstrate the swelling-induced formation of cone-like shapes, where the buckling direction of each unit can be programmed through local variations in Δ. This trilayer concept provides a simple way to simultaneously control both the Gaussian curvature and direction of buckling in shape-morphing hydrogels, with advantages for accessing smaller length-scales compared to existing methods.

Introduction

Materials capable of morphing between two or more programmed three-dimensional (3D) shapes[1-6] have recently garnered significant attention in contexts including artificial swimmers,[7,8] soft robotics,[9,10] biomedical devices,[11,12] biomimetic systems,[13-15] and mechanical metamaterials.[16] Out-of-plane buckling induced by non-uniform deformation in 2D film allows for relatively simple and scalable fabrication of 3D objects.[4-6] To this end, three kinds of stimuli responsive polymer systems—hydrogels,[17] liquid crystal polymers (LCPs),[18] and shape memory polymers (SMPs)[19]—have been extensively studied for shape-morphing materials due to their large deformation ratios, fast response, and/or responses to a variety of stimuli.

Two key approaches are used for the construction of 3D objects from thin 2D sheets: i) control of mean curvature H by introducing *through-thickness* variations and ii) control of Gaussian curvature K by introducing *in-plane* variations in deformation.[4,5] Bilayer bending is a well-known and simple example where through-thickness variations in strain will cause an initially planar sheet to bend into a cylindrical configuration with mean curvature (i.e., the average of the two principal curvatures, where in this case one of the two curvatures is zero) dictated by the mismatch in modulus, thickness, and deformation of the two layers.[20-22] To control Gaussian curvature K (i.e., the product of the two principal curvatures, which varies from positive for sphere-like, elliptic shapes, to negative for saddle-like, hyperbolic shapes), various approaches have been developed to program in-plane variations in deformation including photo-lithographic patterning of hydrogels,[23-25] extruding shear-aligning composite hydrogel inks,[26] printing light-absorbing ink on heat shrink films,[27] and controlling the director orientation within LCPs,[28-32] providing access to a wide range of shapes.

Though a substantial number of material systems and approaches have been developed to control either H or K separately, the simultaneous control of both is far less explored, despite its importance for uniquely selecting 3D shapes. For example, several groups have demonstrated the patterning of arrays of positive K (cone- or sphere-like) features through in-plane variations, but found that multiple different 3D configurations can be adopted, corresponding to each of the positive K features buckling either upward ($H < 0$) or downward ($H > 0$).[23,28,33] A pioneering study by Gladman *et al.* showed how simultaneous control of H and K could be achieved in 3D printed bilayers of composite hydrogels, where the direction of the print path independently controlled the direction of anisotropic swelling in each layer.[26] While quite powerful, this 3D printing method has so far been limited to overall sample dimensions of several cm (yielding fairly slow changes in shape in response to stimuli), and is also challenging to generalize to parallel processing of multiple objects simultaneously. Subsequently, Aharoni *et al.*[34] and Plucinsky *et al.*[35] controlled both H and K within LCP sheets by controlling the rotation of the director field through the film thickness. However, the overall sizes of the 3D

[a] *Department of Polymer Science and Engineering, Kumoh National Institute of Technology, Gumi, Gyeongbuk 39177, South Korea.*
[b] *Department of Polymer Science and Engineering, University of Massachusetts Amherst, Amherst 01003, Massachusetts, USA. E-mail: hayward@umass.edu*

† Footnotes relating to the title and/or authors should appear here.
Electronic Supplementary Information (ESI) available: [details of any supplementary information available should be included here]. See DOI: 10.1039/x0xx00000x

Please do not adjust margins

objects were on the cm-scale as well. For envisioned applications of such materials in biomedical and delivery devices, microfluidic systems, or micro-robotics, it is desirable to develop scalable routes of production of objects with feature sizes in the µm – mm range. Very recently, Zhou *et al.* described the use of through-thickness gradients in crosslink density within thin swellable polymer films to locally bias the direction of buckling, although the reliance on bidirectional photolithographic exposure of films with light penetration depths comparable to the film thickness places significant limitations on the material systems for which this approach is suitable.[36]

Our group has recently developed a platform of hydrogel 'hybrids' consisting of two layers of micro-patterned rigid poly(*para*-methylstyrene) (P*p*MS) elements sandwiching a soft and stimulus-responsive hydrogel sheet.[4,37,38] As the process relies on planar fabrication steps to pattern only three layers, it enables scaling of shape-morphing materials to smaller overall sizes, and potentially to highly parallel processing. Notably, in at least some cases the size-scale of the patterned rigid elements can be several times the film thickness and still lead to an effective 'composite' response of the hybrid material[23,38,39] (in contrast to a traditional composite, where the stiff inclusions are generally orders of magnitude smaller in size than the overall material dimensions). Thus using photolithographic processes with micron-scale resolution, it is possible to successfully pattern films of several micron thickness, and therefore sub-mm-scale lateral dimensions. Further, the extension to high resolution lithographic methods with ~ 100 nm feature sizes presents a clear route to further scale down the sample dimensions in the future.

To date, we have demonstrated that this platform provides access to self-folding origami structures by locally defining gel/P*p*MS bilayer regions of controlled *H* within sheets of otherwise uniform trilayers.[37,40] In addition, we have shown that patterning rigid stripes with crossed orientations on either side of the gel film yields helical structures[38] as well-known for many systems exhibiting 'incompatible curvatures'.[26,30,41,42] We note that a related approach based on patterned stiff elements in swellable gel layers has been developed by Gracias, Nguyen, and co-workers, but has so far been limited to bilayers that do not allow for control of buckling in both upward and downward directions.[43] Here, we show that trilayers with patterns of stripes oriented in parallel, but with varying lateral width, on the two surfaces, allows for simultaneous programming of both the direction of buckling and *K* within simple canonical geometries consisting of multiple cone-like features.

Experimental

Synthesis of photo-crosslinkable glassy polymer

Polymers were synthesized by free-radical polymerization following procedures described previsouly[44] and summarized as follows. Amounts of 3 mL of *para*-methylstyrene (*p*MS), 295 mg of acrylamidobenzophenone (BP), and 15 mg of azobisisobutyronitrile (AIBN) were polymerized in 30 mL of 1,4-dioxane at 80°C for 18 h under nitrogen, resulting in P*p*MS with a BP molar fraction of x = 0.05. AIBN was re-crystallized from methanol prior to use. BP monomer was synthesized via reaction of 4-aminobenzophenone with acryloyl chloride in dichloromethane and triethylamine.[45] The P*p*MS copolymer was purified by precipitation into stirring methanol, washed by filtration, and dried in a vacuum oven overnight. All chemicals were purchased from Aldrich and used as received, except where noted otherwise.

Synthesis of photo-crosslinkable hydrogel 1

Amounts of 3.24 mL of diethylacrylamide (DEAM, TCI), 447 mg of BP, 45 mg of Rhodamine B-labeled methacrylate (RhBMA), and 8.4 mg of AIBN were polymerized in 30 mL of anhydrous 1,4-dioxane at 80°C for 18 h under nitrogen, resulting in PDEAM copolymer with a BP molar fraction of y = 0.07 and a RhB molar fraction of z = 0.003. The PDEAM copolymer was purified by precipitation into stirring hexane, washed by filtration, and dried in a vacuum oven overnight.

Synthesis of photo-crosslinkable hydrogel 2

Amounts of 3.24 mL of DEAM, 60 mg of BP, and 7.8 mg of AIBN were polymerized in 30 mL of anhydrous 1,4-dioxane at 80°C for 18 h under nitrogen, resulting in PDEAM copolymer with comonomer fractions of y = 0.01 and z = 0. The PDEAM copolymer was purified by precipitation into stirring hexane, washed by filtration, and dried in a vacuum oven overnight.

The composition of the P*p*MS and PDEAM copolymers were verified by ^{1}H NMR (Bruker Avance III 500 MHz) as shown in Fig S1.

Fabrication of trilayer structures

Trilayer structures were prepared by sequential spin-coating, crosslinking, and developing of polymer films as described in our prior work[24,37,38,40,46] and illustrated in Fig 1a. We used silicon (Si) wafers as substrates for deposition of polymer layers. Prior to deposition, the Si substrate was washed with water, acetone, and isopropanol for 10 min each in an ultra-sonication bath, and treated with UV-ozone to clean the substrate and raise its surface energy. A thin layer of poly(acrylic acid) (30 kg/mol) crosslinked with Ca^{2+} using $CaCl_2$ was coated on the Si substrate as a sacrificial layer before the trilayer fabrication. For the bottom pattern of rigid lines, a 100 mg/mL P*p*MS solution in toluene was spin-coated at 900 rpm for 1 min, leading to a thickness of ≈ 1 µm. For the hydrogel layer, 100 µL of a 0.75 wt% solution of a 3.5:1 mixture of PDEAM copolymers **1** and **2** was placed on the substrate and evaporated for 5 h at 45°C in a nearly closed glass bottle, leading to a thickness of ≈ 10 µm. This thickness is sufficiently thin to provide rapid swelling and substantial curvature within sub-mm-sized gels, yet requires only ~ 10 µm-scale lithographic resolution, which can easily be achieved using the microscope projection lithography system described below. For the top stripes, spin-coating of a 75 mg/mL P*p*MS-BP solution in toluene at 3000 rpm for 1 min resulted in a layer with the same thickness as the bottom line patterns, ≈ 1 µm, chosen to provide nearly the tightest possible curvatures, while almost completely locally restricting swelling, given the 10 µm hydrogel layer thickness.[37] The thickness of each layer was measured by a stylus profilometer (Dektak, Veeco). The bottom

 This journal is © The Royal Society of Chemistry 20xx

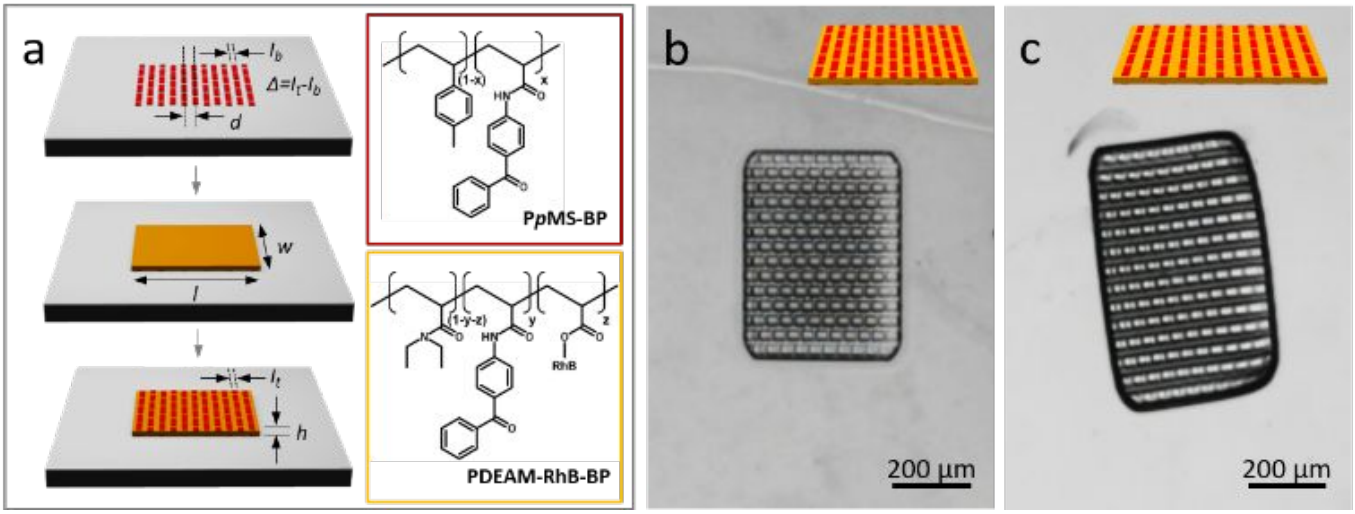

Figure 1 (a) An illustration of the trilayer fabrication process and chemical structures of P*p*MS and PDEAM copolymers (respectively denoted by red and yellow colors). Optical microscope images of a fabricated trilayer structure with uniformly oriented stripes and $\Delta = 0$ (b) in the deswelled state at 60˚C and (c) in the swelled state at 10˚C. An anisotropic swelling ratio of 1.17 is achieved.

P*p*MS layer was exposed to UV to form stripes, followed by developing with a 1:0.65 (vol.) solution of toluene and hexane to remove uncrosslinked regions. The thick middle layer of PDEAM was coated on top of the patterned P*p*MS film and exposed to UV. The PDEAM film was developed using a fresh 1: 0.65 (vol.) solution of toluene and hexane. The top P*p*MS layer was spin coated on top of the PDEAM layer and, followed by UV crosslinking and development using a similar procedure.

Crosslinking was conducted using a pattern of UV light (365 nm, pE-100, CoolLED) generated using a digital micromirror device (DLP discovery 4100, 0/7 XGA, Texas instruments) attached to an inverted optical microscope (Nikon ECLIPSE Ti) with a 10x objective lens (S Fluor, Nikon). A large dose of UV (16 J/cm^2) was used to fully crosslink each film.

Characterization

The fabricated trilayer structures were released from the substrate using a buffered aqueous solution (pH 7.2 phosphate buffer; 1 x 10^{-3} M NaCl) and observed using a Zeiss AxioTech Vario upright microscope with a 5x objective lens. To observe the thermally-responsive behaviour, a temperature stage (Instec HCS612V) with liquid nitrogen cooling was used. For the identification of the buckling direction of cones, 3D reconstructed images were obtained using a confocal microscope (Nikon A1+) with a 10x objective lens and a 561 nm laser source for excitation of Rhodamine B fluorescence. Lengths for the determination of the anisotropic swelling ratio were measured using Image J software.

Results and discussion

Trilayer structures of P*p*MS/PDEAM/P*p*MS are fabricated by sequential spin coating, crosslinking, and developing of polymer films as illustrated in Fig 1a. The use of PDEAM, as in our previous work on fabrication of helices,[38] offers the advantage of more rapid swelling/deswelling kinetics compared to the poly(*N*-isopropyl acrylamide) copolymers used previously for patterning swelling of single layer hydrogels.[23] Single-layer hydrogel samples lacking P*p*MS show isotropic swelling by a linear factor of 1.65 in both directions (Fig S2). This value is achieved by mixing the two PDEAM copolymers **1** and **2**, containing different content of the photo-crosslinkable BP groups, in a mass ratio of 1:3.5.

We first consider the behaviour of rectangular trilayer samples with in plane dimensions of 400 x 550 μm^2 and gel layer thickness (*h*) of 10 μm, as shown in Fig 1b-c. Uniformly oriented dashed P*p*MS stripes with a centre-to-centre spacing of d = 40 μm are patterned on both sides. The uniform orientation of stripes is chosen to yield anisotropic in-plane expansion without encoding any Gaussian curvature. The use of dashed (with respective dash and gap lengths of 109 μm and 22 μm, such that the gaps occupy a fraction of the line length of 0.17) rather than continuous P*p*MS lines is motivated by difficulties in programming non-zero *K* shapes with continuous stripes, as described in more detail below. We note that the value of d/h = 4 is chosen based on our previous studies indicating critical values of $d/h \approx 5$ and 8 to achieve composite-type responses for single gel layers with patterned stripes[39] and circular dots,[23] respectively (where larger values of d/h yielded buckling on the scale of the micro-patterns). Indeed, as shown in Fig 1c, the patterned trilayers with d/h = 4 remain globally flat upon swelling, consistent with a composite response. For this sample, the lateral width of the stripes on the top l_t, and bottom l_b, is kept equal at 22 μm, corresponding to a difference of $\Delta = l_t - l_b = 0$. In addition, the thickness t of the stripes is matched at 1 μm on both sides to make the samples as symmetric as possible. For samples with d/h substantially larger than 5, sheets were found to curve around the axis perpendicular to the stripes due to the effective in-plane variations in swelling, as described in detail in our previous work on single gel layers with patterned stiff stripes.[36]

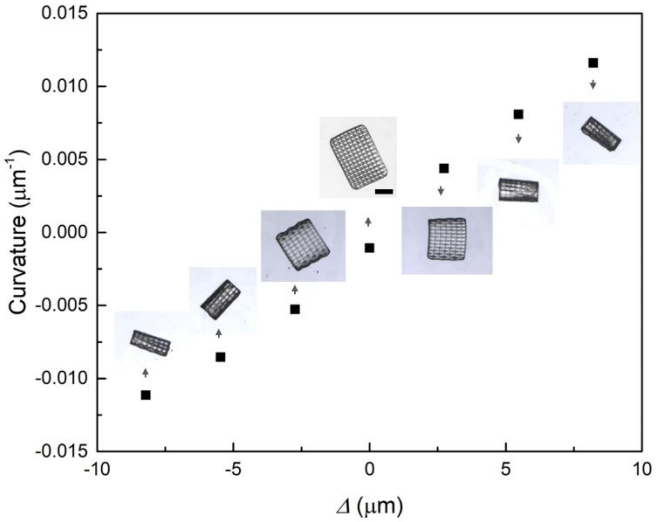

Figure 2 Curvature obtained at 10°C is plotted against Δ. Insets are optical microscope images of the trilayer structures in the swelled state corresponding to each data point. The scale bar is 200 μm.

As shown in Mov S1, such a patterned trilayer structure exhibits anisotropic swelling but otherwise remains nearly flat throughout a cycle first deswelling by heating to 60°C and subsequently reswelling by cooling to 10°C. The characteristic time required in both cases is of order minutes, however as this is similar to the time required for the sample to reach the set temperature, we expect that the intrinsic response rate is likely somewhat faster. Comparing the dimensions in the swelled (Fig 1c) and deswelled (Fig 1b) states, we determine overall swelling ratios of 1.28 and 1.09 along the directions perpendicular, and parallel, to the stripes, respectively. These swelling ratios are very close to the values of 1.29 and 1.10 estimated simply (ignoring effects of Poisson's ratio) by weighting the linear swelling of the PDEAM layer alone (1.65) by the fraction of PDEAM perpendicular to (0.45) and along (0.17) the stripes, respectively, and assuming that the P*p*MS coated stripes do not deform. This represents a swelling anisotropy of 1.17, similar to the values achieved previously for single layer gels with patterned stiff regions by Byun *et al.*,[39] and for oriented composite hydrogels by Gladman *et al.*[26] Presumably, however, somewhat greater anisotropy should be possible in the future by either reducing the widths of the stripes (at constant spacing) or increasing the swelling of the PDEAM layer by using a lesser content of polymer **1**.

Having demonstrated anisotropic in-plane expansion of trilayers with uniformly oriented and symmetric rigid lines, we next consider the ability to control the direction and magnitude of curvature by introducing an offset in the line width from the top to bottom surface, i.e., $\Delta \neq 0$. Specifically, we keep the average line width constant at 22 μm and vary Δ progressively from -8.2 to +8.2 μm, as summarized in Fig 2. For negative Δ, the top surface of the gel seeks to swell more than the bottom side, giving rise to upward buckling (with the gel centre rising above the edges; negative H) into a cylindrical configuration. In contrast, positive Δ leads to downward buckling (positive H). As seen in Fig 2, the resulting curvature increases monotonically

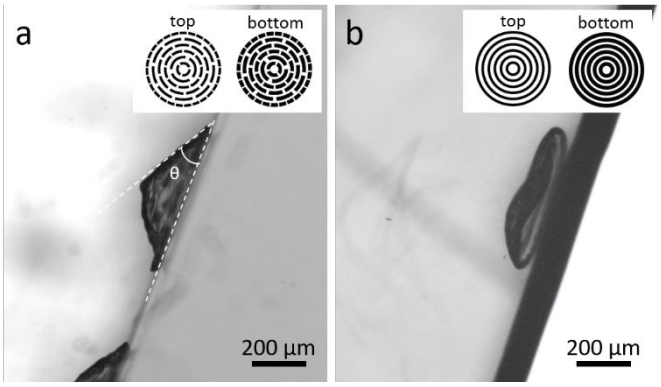

with increasing Δ, with rather tight curvatures of H = -0.011 and +0.012 μm^{-1} for Δ = -8.2 and +8.2 μm, respectively. Using the same approach as above to estimate the linear swelling along the direction perpendicular to the stripes yields a mismatch strain ε of 0.13 between the two surfaces for the largest magnitude of Δ studied. From the geometric relationship $R^{-1} = \varepsilon h^{-1}$, this would correspond to an expected curvature of $|H| = 0.008$ μm^{-1}, where here h represents the thickness of the gel in the swelled state, which is in reasonable agreement with the measured values given that the strains are not very small. For $\Delta = 0$, a slight negative curvature, -1.07×10^{-3} μm^{-1}, is observed, presumably due to slight differences in thickness between the top and bottom P*p*MS lines or a small residual stress gradient within the PDEAM layer.

Taking advantage of the ability to control curvature through variations in Δ, we next turn to a simple demonstration of simultaneous programming of both buckling direction and K. We introduce concentric P*p*MS line patterns on both sides of PDEAM; this arrangement should provide greater swelling in the radial than the azimuthal direction, defining a cone (with a positive K singularity at its tip) as the target shape, as has been widely studied for LCPs with concentric orientation of the director.[28-32] We set the diameter of the n-th ring out from the centre as $82 \cdot n$ μ m, providing a constant spacing between adjacent rings of 41 μm. But, due to asymmetricity in P*p*MS line widths, we can control buckling direction of a cone according to the sign of Δ, positive or negative. For example, Δ = -8.2 μm causes upward buckling direction and Δ = +8.2 μm causes downward buckling direction. To confirm the upward buckling for Δ = -8.2 μm, the cone is carefully moved to an edge of the silicon wafer using a sharp tip end and made to tilted 90° by leaning it against the edge (Fig 3a). The angle of the cone measured from Fig 3a, 31°, is consistent with that of the target cone angle of $\cos^{-1}(1.09/1.28) = 32°$ calculated from the swelling anisotropy. Although buckling does occur in the designed direction, we note that the mechanism of selection is not completely understood, since the programmed *direction* of

Figure 3 (a) A side view optical microscope image of a cone fabricated from the trilayer structure composed of concentric dashed line patterns (inset schematic) of P*p*MS with an offset of Δ = -8.2 μm. The cone angle θ is 31°. (b) An optical microscope image of the distorted shape formed by a similar trilayer structure but with continuous lines of P*p*MS on each surface.

This journal is © The Royal Society of Chemistry 20xx

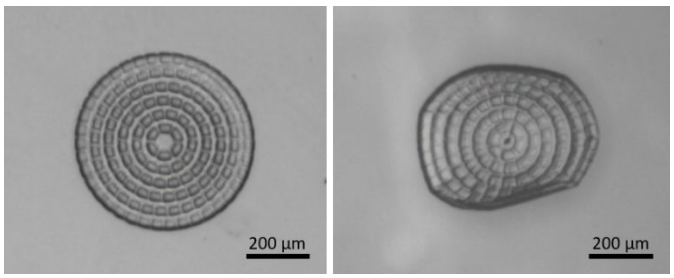

Figure 4 Optical microscope images of a trilayer structure with dashed concentric circles of P*p*MS with constant dash and gap lengths (a) in the deswelled state at 60°C and (b) in the swelled state at 10 °C, where bending is observed instead of the formation of a cone.

preferred curvature is transverse to the rigid stripes, whereas in the realized cone, the curvature is along the striped direction. Interestingly, when we attempt to pattern a cone shape using continuous, rather than dashed, lines of P*p*MS, the distorted shape shown in Fig 3b (and in Mov S2 as a series of images with different tilt angles) is observed instead. We interpret this configuration as being nearly conical, but with a portion of the cone buckled upward and the remaining portion buckled downward. We suspect that this departure from the target shape results from the very high bending stiffness of the trilayer film regions, whereas the introduction of gaps in the stripes lowers the effective bending modulus.

Even when using dashed lines, a careful consideration of the arrangements of dashes and gaps is necessary to achieve the target shape. For example, Fig 4a shows a disk in the deswelled state patterned using respective fixed dash and gap lengths of 35.8 and 7.2 μm, corresponding to 6 dashes in the innermost circle. To minimize alignment between gaps in neighbouring rings on the same surface, every successive ring is azimuthally offset by 15˚ (such that each gap in the 2nd ring aligned with the centre of a dash in the 1st.) The P*p*MS dashes on the top and bottom surface are azimuthally offset by 15˚, which prevent alignment between gaps on opposing surfaces except for gaps in the 4th ring from centre. By providing an additional azimuthal offset of 7.5˚ between the 4th ring on the top and bottom surfaces, alignment between gaps on opposing surfaces is completely avoided (Fig S3). Despite these efforts, however, as seen in Fig 4b, upon swelling, the disk curls into a roughly cylindrical shape, rather than adopting the target conical shape, and also shows some regions of higher localized curvature. This behaviour appears to arise due to alignment between gaps on neighbouring rings (see Fig S3a), which can yield a locally 'softer' region of the disk that accommodates swelling through localized deformation, thereby distorting the global shape change. To avoid such issues, we develop a simple algorithm for patterning dashes and gaps. Specifically, as illustrated in Fig S4, we begin with 3 dashes with lengths of 71.3 and gaps of 14.6 μm along the innermost circle (preserving the gap fraction of 0.17), with the patterns offset by an azimuthal angle of 60˚ from the top to bottom surface, to ensure that these gaps are anti-aligned. Similarly, the dashes in the second ring out from the centre are rotated by 60˚ relative to the innermost ring, preventing lateral alignment, while both dashes and gaps are increased proportionally in length. This procedure is repeated until the lengths of dashes in a given ring would exceed 109 μm (a somewhat arbitrary choice, but one based on our experience with swelling of the sheets with uniformly oriented stripes in Fig 1), at which point the number of stripes is increased 3-fold to 9, and the angular offsets are similarly reduced to 20˚. This algorithm can then be repeated to yield arbitrarily large rings while ensuring that gaps do not align between neighbouring rings or from the top to bottom surfaces. Such considerations are presumably necessary because the length-scales of the patterned stiff elements are very close to the limit where the system behaves as an effective composite. Although this complicates the design of pattern geometries, in light of the potential advantages for reducing the overall size-scales of shape-morphing materials, we believe that further studies into the response of such discretely-patterned hybrid materials with more complex pattern geometries is well justified. Finally, we prepare samples designed to buckle into three cones in a row to demonstrate control of the buckling direction of each cone. For example, Fig 5a shows a sample in the deswelled state where Δ is set as -8.2 μm / +8.2 μm / -8.2 μm for the three cones, corresponding to a target shape with upward / downward / upward buckling directions. We denote the regions programmed to buckle upward and downward with red and blue colouring, respectively, in Fig 5a, while the grey regions are not programmed with any preferred mean curvature (i.e., $\Delta = 0$ μm). Upon swelling the sample does indeed adopt the programmed configuration, as verified by the 3D reconstruction from confocal fluorescence microscopy in Fig 5b, and Mov S3 showing bright field images during swelling of a sample that remains attached to the substrate along one edge. Similarly, when we set Δ as +8.2 μm / +8.2 μm / -8.2 μm for the three cones, the sample swells into a shape with downward / downward / upward buckling directions, as shown in Fig 5c.

Conclusions

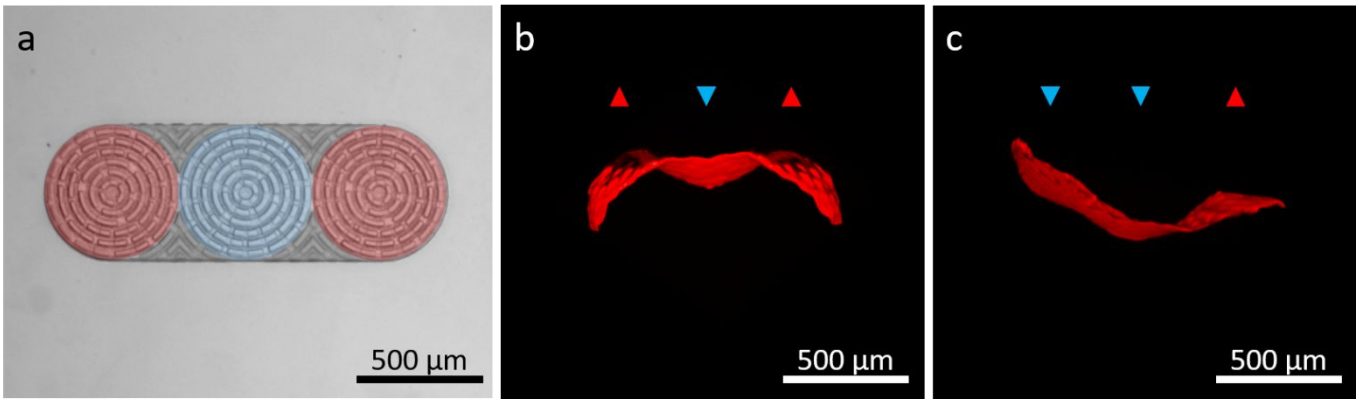

Figure 5 (a) An optical microscope image of a trilayer sheet in the deswelled state at 60°C consisting of three connected regions programmed to buckle into conical shapes with upward (left) / downward (middle) / upward (right) directions. Regions programmed with negative (red; Δ = -8.2 µm) and positive (blue; Δ = +8.2 µm) curvature are indicated, while the remaining regions are programmed with no mean curvature (Δ = 0 µm). (b) A side view image of the same sample as (a) but in the swelled state at 10°C from a 3D reconstructed confocal fluorescence image showing the targeted buckling configuration. (c) A side view confocal image of a sample of three connected cones programmed to have downward (left) / downward (middle) / upward (right) buckling directions.

Hydrogel hybrids composed of patterned rigid stripes of a glassy polymer, P*p*MS, sandwiching a temperature-responsive PDEAM hydrogel film were prepared by a three-layer photolithographic process. For all experiments, dashed, rather than continuous, lines of P*p*MS were employed to reduce the effective bending stiffness of the multilayer films. When the stripes on the top and bottom surfaces were uniformly oriented and had the same widths on the top and bottom surfaces, the trilayers underwent anisotropic expansion. By introducing an offset Δ in the line widths, it was possible to control both the direction of buckling and the magnitude of mean curvature for uniformly oriented stripe patterns. For the case of circular disks patterned with concentric stripes, swelling of the gel led to formation of conical shapes, which could be programmed to buckle upward or downward for negative or positive values of Δ, respectively. As a simple demonstration of patterns containing spatial variations in both mean and Gaussian curvature, we fabricated sets of three cones connected in a row, and demonstrated the independent control of the buckling direction for each cone by local variations in the sign of Δ. For advanced approaches to shape-morphing materials, the ability to simultaneously control both mean and Gaussian curvature is an essential feature. The trilayer approach provides a simple approach to achieve such control, on substantially smaller length-scales than has previously been possible.

Conflicts of interest

There are no conflicts to declare.

Acknowledgements

This work was supported by the US Army Research Office through grant W911NF-16-1-0119. Additional support for data analysis and manuscript preparation was given by the National Research Foundation of Korea (NRF) grant funded by the Korea Government (NRF-2018R1D1A1B07044075).

References

1. L. Ionov, *Langmuir*, 2015, **31**, 5015-5024.
2. J. Rogers, Y. Huang, O. G. Schmidt, and David H. Gracias, *MRS Bull.*, 2016, **41**, 123-129.
3. Y. Liu, J. Genzer, and M. D. Dickey, *Prog. Poly. Sci.*, 2016, **52**, 79-106.
4. S.-J. Jeon, A. W. Hauser, and R. C. Hayward, *Acc. Chem. Res.*, 2017, **50**, 161-169.
5. T. van Manen, S. Janbaz, and A. A. Zadpoor, *Mater. Today.*, 2018, **21**, 144-163.
6. A. B. Baker, S. R. G. Bates, T. M. Llewellyn-Jones, L. P. B. Valori, M. P. M. Dicker, and R. S. Trask, *Mater. Des.*, 2019, **163**, 107544.
7. S. Palagi, A. G. Mark, S. Y. Reigh, K. Melde, T. Qiu, H. Zeng, C. Parmeggiani, D. Martella, A. Sanchez-Castillo, N. Kapernaum, F. Giesselmann, D. S. Wiersma, E. Lauga, and P. Fischer, *Nat. Mater.*, 2016, **15**, 647-654.
8. J. J. Wie, M. R. Shankar, and T. J. White, *Nat. Commun.*, 2016, **7**, 13260.
9. H. Zeng, P. Wasylczyk, D. S. Wiersma, and A. Priimagi, *Adv. Mater.*, 2018, **30**, 1703554.
10. S. Palagi and P. Fischer, *Nat. Rev. Mater.*, 2018, **3**, 113-124.
11. Y. Qiu and K. Park, *Adv. Drug. Delivery Rev.*, 2012, **64**, 49-60.
12. H. R. Culver, J. R. Clegg, and N. A. Peppas, *Acc. Chem. Res.*, 2017, **50**, 170-178.
13. R. Kempaiah and Z. Nie, *J. Mater. Chem. B*, 2014, **2**, 2357-2368.
14. J. A. Faber, A. F. Arrieta, and A. R. Studart, *Science*, 2018, **359**, 1386-1391.
15. H. Shahsavan, L. Yu, A. Jákli, and B. Zhao, *Soft Matter*, 2017, **13**, 8006-8022.
16. H. Zhang, X. Guo, J. Wu, D. Fang, and Y. Zhang, *Sci. Adv.*, 2018, **4**, eaar8535.
17. S.-K. Ahn, R. M. Kasi, S.-C. Kim, N. Sharma, and Y. Zhou, *Soft Matter*, 2008, **4**, 1151-1157.
18. B. A. Kowalski, T. C. Guin, A. A. Auguste, N. P. Godman, and T. J. White, *ACS Macro Lett.*, 2017, **6**, 436-441.
19. H. Meng and G. Li, *Polymer*, 2013, **54**, 2199-2221.
20. G. G. Stoney, *Proc. R. Soc. London., Ser. A,* 1909, **82**, 172-175.
21. S. Timoshenko, *J. Opt. Soc. Am.*, 1925, **11**, 233-255.
22. Z. Hu, X. Zhang, and Y. Li, *Science*, 1995, **269**, 525-527.

This journal is © The Royal Society of Chemistry 20xx

23. J. Kim, J. A. Hanna, M. Byun, C. D. Santangelo, and R. C. Hayward, *Science*, 2012, **335**, 1201-1205.
24. J.-H. Na, N. P. Bende, J. Bae, C. D. Santangelo, and R. C. Hayward, *Soft Matter*, 2016, **12**, 4985-4990.
25. Z. L. Wu, M. Moshe, J. Greener, H. Therien-Aubin, Z. Nie, E. Sharon, and E. Kumacheva, *Nat. Commun.* 2013, **4**, 1586.
26. A. S. Gladman, E. A. Matsumoto, R. G. Nuzzo, L. Mahadevan, and J. A. Lewis, *Nat. Mater.*, 2016, **15**, 413-418.
27. A. M. Hubbard, R. W. Mailen, M. A. Zikry, M. D. Dickey, and J. Genzer, *Soft Matter*, 2017, **13**, 2299-2308.
28. T. H. Ware, M. E. McConney, J. J. Wie, V. P. Tondiglia, and T. J. White, *Science*, 2015, **347**, 982-984.
29. A. Kotikian, R. L. Truby, J. W. Boley, T. J. White, and J. A. Lewis, *Adv. Mater.*, 2018, **30**, 1706164.
30. S. Iamsaard, S. J. Aβhoff, B. Matt, T. Kudernac, J. J. L. M. Cornelissen, S. P. Fletcher, and N. Katsonis, *Nat. Chem.*, 2014, **6**, 229.
31. C. D. Modes, K. Bhattacharya, and M. Warner, *Phys. Rev. E*, 2010, **81**, 060701.
32. L. T. de Haan, C. Sánchez-Somolinos, C. M. W. Bastiaansen, A. P. H. J. Schenning, and D. J. Broer, *Angew. Chem. Int. Ed.*, 2012, **51**, 12469-12472.
33. Z. J. Wang, W. Hong, Zi Liang Wu, and Q. Zheng, *Angew. Chem. Int. Ed.*, 2017, **56**, 15974-15978.
34. H. Aharoni, Y. Xia, X. Zhang, R. D. Kamien, and S. Yang, *Proc. Natl. Acad. Sci. U.S.A.*, 2018, **115**, 7206-7211.
35. P. Plucinsky, B. A. Kowalski, T. J. White, and K. Bhattacharya, *Soft Matter*, 2018, **14**, 3127-3134.
36. Y. Zhou, C. M. Duque, C. D. Santangelo, and R. C. Hayward, *Adv. Funct. Mater.*, 2019, DOI: 10.1002/adfm.201905273.
37. J.-H. Na, A. A. Evans, J. Bae, M. C. Chiappelli, C. D. Santangelo, R. J. Lang, T. C. Hull, and R. C. Hayward, *Adv Mater.*, 2015, **27**, 79-85.
38. S.-J. Jeon and R. C. Hayward, *Adv. Mater.*, 2017, **29**, 1606111.
39. M. Byun, C. D. Santangelo, and R. C. Hayward, *Soft Matter*, 2013, **9**, 8264-8273.
40. J. L. Silverberg, J.-H. Na, A. A. Evans, B. Liu, T. C. Hull, C. D. Santangelo, R. J. Lang, R. C. Hayward, and I. Cohen, *Nat. Mater.*, 2015, **14**, 389-393.
41. Y. Klein, E. Efrati, and E. Sharon, *Science*, 2007, **315**, 1116-1120.
42. R. M. Erb, J. J. Sander, R. Grisch, and A. R. Studart, *Nat. Commun.*, 2013, **4**, 1712.
43. J. Guo, T. Shroff, C. Yoon, J. Liu, J. C. Breger, D. H. Gracias, and T. D. Nguyen, *Extreme Mech. Lett.*, 2017, **16**, 6-12.
44. S. K. Christensen, M. C. Chiappelli, and R. C. Hayward, *Macromolecules*, 2012, **45**, 5237-5246.
45. J. Jia, M. Sarker, M. G. Steinmetz, R. Shukla, and R. J. Rathore, *J. Org. Chem.*, 2008, **73**, 8867-8879.
46. S.-J. Jeon, M. C. Chiappelli, and R. C. Hayward, *Adv. Funct. Mater.*, 2016, **26**, 722-728.

This journal is © The Royal Society of Chemistry 20xx